ViPR: Visual-Odometry-aided Pose Regression for 6DoF Camera Localization

Felix Ott[1], Tobias Feigl[1,2], Christoffer Löffler[1,2], and Christopher Mutschler[1,3]

[1]Fraunhofer Institute for Integrated Circuits IIS, Nuremberg, Germany
[2]Department of Computer Science, FAU Erlangen-Nuremberg, Germany
[3]Department of Statistics, Ludwig-Maximilians-University (LMU), Munich, Germany
{felix.ott | tobias.feigl | christoffer.loeffler | christopher.mutschler}@iis.fraunhofer.de

Abstract

Visual Odometry (VO) accumulates a positional drift in long-term robot navigation tasks. Although Convolutional Neural Networks (CNNs) improve VO in various aspects, VO still suffers from moving obstacles, discontinuous observation of features, and poor textures or visual information. While recent approaches estimate a 6DoF pose either directly from (a series of) images or by merging depth maps with optical flow (OF), research that combines absolute pose regression with OF is limited.

We propose ViPR, a novel modular architecture for long-term 6DoF VO that leverages temporal information and synergies between absolute pose estimates (from PoseNet-like modules) and relative pose estimates (from FlowNet-based modules) by combining both through recurrent layers. Experiments on known datasets and on our own Industry dataset show that our modular design outperforms state of the art in long-term navigation tasks.

1. Introduction

Real-time tracking of mobile objects (e.g., forklifts in industrial areas) allows to monitor and optimize workflows and tracks goods for automated inventory management. Such environments typically include large warehouses or factory buildings, and localization solutions often use a combination of radio-, LiDAR- or radar-based systems, etc.

However, these solutions often require infrastructure or they are costly in their operation. An alternative approach is a (mobile) optical pose estimation based on ego-motion. Such approaches are usually based on SLAM (Simultaneous Localization and Mapping), meet the requirements of exact real-time localization, and are also cost-efficient.

Available pose estimation approaches are categorized into three groups: classical, hybrid, and deep learning (DL)-based methods. Classical methods often require an infrastructure that includes either synthetic (i.e., installed in the environment) or natural (e.g., walls and edges) markers. The accuracy of the pose estimation depends to a large extent on suitable invariance properties of the available features such that they can be reliably recognized. However, to reliably detect features, we have to invest a lot of expensive computing time [38, 27]. Additional sensors (e.g., inertial sensors, depth cameras, etc.) or additional context (e.g., 3D models of the environment, prerecorded landmark databases, etc.) may increase the accuracy but also increase system complexity and costs [44]. Hybrid methods [66, 7, 6, 23, 74] combine geometric and machine learning (ML) approaches. For instance, ML predicts the 3D position of each pixel in world coordinates, from which geometry-based methods infer the camera pose [16].

Recent DL approaches partly address the above mentioned issues of complexity and cost, and also aim for high positioning accuracy, e.g., regression forests [51, 74] learn a mapping of images to positions based on 3D models of the environment. Absolute pose regression (APR) uses DL [63] as a cascade of convolution operators to learn poses only from 2D images. The pioneer PoseNet [33] has been extended by Bayesian approaches [31], long short-term memories (LSTMs) [77] and others [50, 26, 36, 11]. Recent APR methods such as VLocNet [72, 59] and DGRNets [42] introduce relative pose regression (RPR) to address the APR-

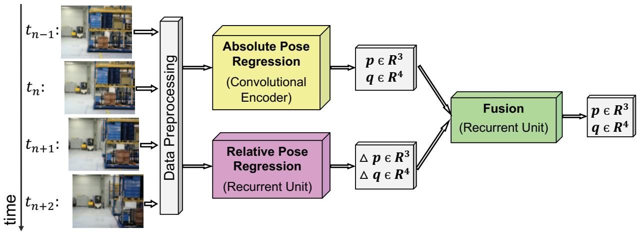

Figure 1: Our pose estimation pipeline solves the APR- and RPR-tasks in parallel, and recurrent layers estimate the final 6DoF pose.

2160-7516/20/$31.00 ©2020 IEEE
DOI 10.1109/CVPRW50498.2020.00029

task. While APR needs to be trained for a particular scene, RPR may be trained for multiple scenes [63]. However, RPR alone does not solve the navigation task.

For applications such as indoor positioning, existing approaches are not yet mature, i.e., in terms of robustness and accuracy to handle real-world challenges such as changing environment geometries, lighting conditions, and camera (motion) artifacts. This paper proposes a modular fusion technique for 6DoF pose estimation based on a PoseNet-like module and predictions of a relative module for VO. Our novel relative module uses the flow of image pixels between successive images computed by FlowNet2.0 [25] to capture time dependencies in the camera movement in the recurrent layers, see Fig. 1. Our model reduces the positioning error using this multitasking approach, which learns both the absolute poses based on monocular (2D) imaging and the relative motion for the task of estimating VO.

We evaluate our approach first on the small-scale 7-Scenes [66] dataset. As other datasets are unsuitable to evaluate continuous navigation tasks we also release a dataset that can be used to evaluate various problems arising from real industrial scenarios such as inconsistent lighting, occlusion, dynamic environments, etc. We benchmark our approach on both datasets against existing approaches [33, 77] and show that we consistently outperform the accuracy of their pose estimates.

The rest of the paper is structured as follows. Section 2 discusses related work. Section 3 provides details about our architecture. We discuss available datasets and introduce our novel *Industry* dataset in Section 4. We present experimental results in Section 5 before Section 6 concludes.

2. Related Work

SLAM-driven 3D point registration methods enable precise self-localization even in unknown environments. Although VO has made remarkable progress over the last decade, it still suffers greatly from scaling errors of real and estimated maps [43, 69, 49, 29, 34, 35, 40, 54, 4, 39]. With more computing power, Visual Inertial SLAM combines VO with Inertial Measurement Unit (IMU) sensors to partly resolve the scale ambiguity, to provide motion cues without visual features [43, 70, 29], to process more features, and to make tracking more robust [69, 34]. Multiple works combine global localization in a scene with SLAM/(Inertial) VO [46, 17, 55, 64, 22, 52, 28]. However, recent SLAM methods do not yet meet industry-strength with respect to accuracy and reliability [57, 18] as they need undamaged, clean and undisguised markers [39, 30] and as they still suffer from long-term stability and the effects of movement, sudden acceleration and occlusion [75]. SIFT-like point-based features [45] for the localization from landmarks [3, 24, 41, 78] require efficient retrieval methods, use VLAD encodings such as DenseVLAD [71], use anchor points such as AnchorNet [60], or use RANSAC-based optimization such as DSAC [6] and ActiveSearch [61].

VO primarily addresses the problem of separating ego-from feature-motion and suffers from area constraints, poorly textured environments, scale drift, a lack of an initial position, and thus inconsistent camera trajectories [10]. Instead, PoseNet-like architectures (see Sec. 2.1) that estimate absolute poses on single-shot images are more robust, less compute-intensive, and can be trained in advance on application data. Unlike VO, they do not suffer from a lack of initial poses and do not require access to camera parameters, good initialization, and handcrafted features [65]. Although the joint estimation of relative poses may contribute to increasing accuracy (see Sec. 2.2), such hybrid approaches still suffer from dynamic environments, as they are often trained offline in quasi-rigid environments. While optical flow (see Sec. 2.3) addresses these challenges it has not yet been combined with APR for 6DoF self-localization.

2.1. Absolute Pose Regression (APR)

Methods that derive a 6DoF pose directly from images have been studied for decades. Therefore, there are currently many classic methods whose complex components are replaced by machine learning (ML) or DL. For instance, RelocNet [2] learns metrics continuously from global image features through a camera frustum overlap loss. CamNet [15] is a coarse (image-based)-to-fine (pose-based) retrieval-based model that includes relative pose regression to get close to the best database entry that contains extracted features of images. NNet [37] queries a database for similar images to predict the relative pose between images and a RANSAC [67] solves the triangulation to provide a position. While those *classic* approaches have already been extended with DL-components their pipelines are expensive as they embed feature matching and projection and/or manage a database. Most recent (and simple) DL-based also outperform their accuracies.

The key idea of PoseNet [33] and its variants [32, 31, 20, 77, 76, 79, 58, 65, 56, 66] among others such as BranchNet [56] and Hourglass [66] is to use a CNN for camera (re-)localization. PoseNet works with scene elements of different scales and is partially insensitive to light changes, occlusions and motion blur. However, while Dense PoseNet [33] crops subimages, PoseNet2 [32] jointly learns network and loss function parameters, [31] links a *Bernoulli* function and applies variational inference [20] to improve the positioning accuracy. However, those variants work with single images, and hence, do not use the temporal context (which is available in continuous navigation tasks), that could help to increase accuracy.

In addition to PoseNet+LSTM [77], there are also similar approaches that exploit time-context that is inherently given by consecutive images (i.e., DeepVO [79],

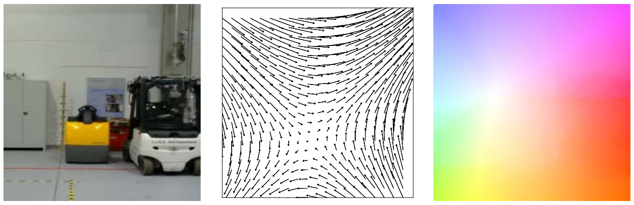

Figure 2: Optical flow (OF): input image (left); OF-vectors as RPR-input (middle); color-coded visualization of OF [1] (right).

ContextualNet [58], and VidLoc [12]). Here, the key-idea is to identify temporal connections in-between the feature vectors (extracted from images) with LSTM-units and to only track feature correlations that contribute the most to the pose estimation. However, there are hardly any long-term dependencies between successive images, and therefore LSTMs give worse or equal accuracy to, for example, simple averaging over successively estimated poses [65]. Instead, we combine estimated poses from time-distributed CNNs with estimates of the OF to maintain the required temporal context in the features of image series.

2.2. APR/RPR-Hybrids

In addition to approaches that derive a 6DoF pose directly from an image there are hybrid methods that combine them with VO to increase the accuracy. VLocNet [72] is closely related to our approach as it estimates a global pose and combines it with VO (but it does not use OF). To further improve the (re-)localization accuracy VLocNet++ [59] uses features from a semantic segmentation. However, we use different networks and do not need to share weights between VO and the global pose estimation. DGRNets [42] estimates both the absolute and relative poses, concatenates them, and uses recurrent CNNs to extract temporal relations between consecutive images. This is similar to our approach but we estimate the relative motion with OF, which allows us to train in advance on large datasets, making the model more robust. MapNet [8] learns a map representation from input data, combines it with GPS, inertial data, and unlabeled images, and uses pose graph optimization (PGO) to combine absolute and relative pose predictions. However, compared to all other methods the most accurate extension of it, MapNet+PGO, does not work on purely visual information, but exploits additional sensors.

2.3. Optical Flow

Typically, VO uses OF to extract features from image sequences. Motion fields, see Fig. 2 (middle), are used to estimate trajectories of pixels in a series of images. For instance, Flowdometry [53] and LS-VO [13] estimate displacements and rotations from OF. [48] proposed a VO-based dead reckoning system that uses OF to match features. [80] combined two CNNs to estimate the VO-motion: FlowNet2-ss [25] estimates the OF and PCNN [14] links two images to process global and local pose information. However, to the best of our knowledge, we are the first to propose an OF-based architecture that estimates the relative camera movement through RNNs, using OF [25].

3. Proposed Model

After a data preprocessing that crops subimages of size $224 \times 224 \times 3$ from a sequence of four images, our pose regression pipeline consists of three parts (see Fig. 3): an APR-network, a RPR-network, and a 6DoF pose estimation (PE) network. PE uses the outputs of the APR- and RPR-networks to provide the final 6DoF pose.

3.1. Absolute Pose Regression (APR) Network

Our APR-network predicts the 6DoF camera pose from three input images based on the original PoseNet [33] model (i.e., essentially a modified GoogLeNet [68] with a regression head instead of a softmax) to train and predict the absolute positions $\boldsymbol{p} \in \mathbb{R}^3$ in the Euclidean space and the absolute orientations $\boldsymbol{q} \in \mathbb{R}^4$ as quaternions. From a single monocular image $\boldsymbol{I}$ the model predicts the pose

$$\tilde{\boldsymbol{x}} = [\tilde{\boldsymbol{p}}, \tilde{\boldsymbol{q}}], \tag{1}$$

as approximations to the actual $\boldsymbol{p}$ and $\boldsymbol{q}$. As the original model learns the image context, based on shape and appearance of the environment, but does not exploit the time context and relation between consecutive images [32], we adapted the model to a *time-distributed* variant. Hence, instead of a single image the new model receives three (consecutive) input images (at timesteps t_{n-1}, t_n, and t_{n+1}), see top part of Fig. 3, uses three separate dense layers (one for each pose) with 2,048 neurons each, and each of the dense layers yields a pose. The middle pose yields the most accurate position for the image at time step t_n.

3.2. Relative Pose Regression (RPR) Network

Our RPR-network uses FlowNet2.0 [25] on each consecutive pairs of the four input images to compute an approximation of the OF (see Fig. 2) and to predict three relative poses for later use. As displacements of similar length but from different camera viewing directions result in different OFs, the displacement and rotation of the camera between pairwise images must be *relative* to the camera's viewing direction of the first image. Therefore, we transform each camera's global coordinate systems (x_n, y_n, z_n) to the same local coordinate system $(\tilde{x}_n, \tilde{y}_n, \tilde{z}_n)$ by

$$\begin{pmatrix} \tilde{x}_n \\ \tilde{y}_n \\ \tilde{z}_n \end{pmatrix} = \boldsymbol{R} \begin{pmatrix} x_n \\ y_n \\ z_n \end{pmatrix}, \tag{2}$$

with the rotation matrix $\boldsymbol{R}$. The displacement $\Delta\tilde{x}_n, \Delta\tilde{y}_n, \Delta\tilde{z}_n$ is the difference between the transformed coordinate systems. The displacement in global coordinates

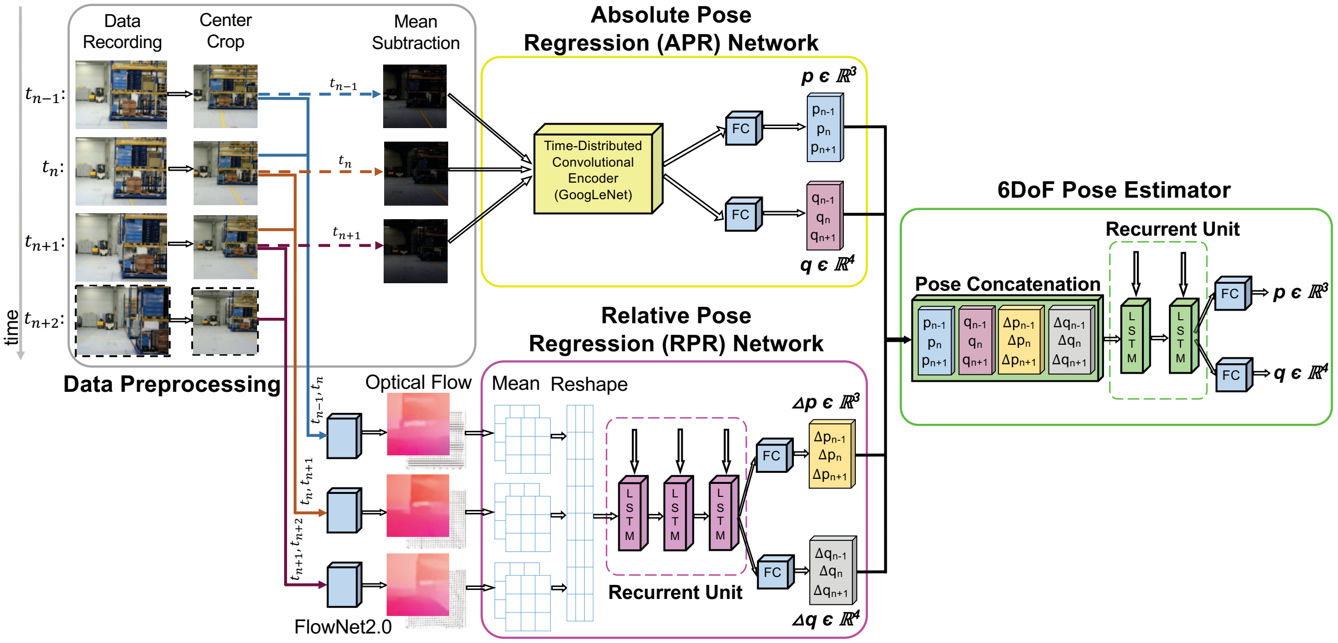
Data Recording
Center Crop
Mean Subtraction
t_{n-1}:
t_n:
t_{n+1}:
t_{n+2}:
time
t_{n-1}
t_n
t_{n+1}
Data Preprocessing
Absolute Pose Regression (APR) Network
Time-Distributed Convolutional Encoder (GoogLeNet)
FC
FC
p ϵ ℝ³
p_{n-1} p_n p_{n+1}
q_{n-1} q_n q_{n+1}
q ϵ ℝ⁴
Relative Pose Regression (RPR) Network
Optical Flow
Mean
Reshape
t_{n-1}, t_n
t_n, t_{n+1}
t_{n+1}, t_{n+2}
LSTM
LSTM
LSTM
Recurrent Unit
FC
FC
Δp ϵ ℝ³
Δp_{n-1} Δp_n Δp_{n+1}
Δq_{n-1} Δq_n Δq_{n+1}
Δq ϵ ℝ⁴
FlowNet2.0
6DoF Pose Estimator
Recurrent Unit
Pose Concatenation
p_{n-1} p_n p_{n+1}
q_{n-1} q_n q_{n+1}
Δp_{n-1} Δp_n Δp_{n+1}
Δq_{n-1} Δq_n Δq_{n+1}
LSTM
LSTM
FC
FC
p ϵ ℝ³
q ϵ ℝ⁴

Figure 3: **Pipeline of the ViPR-architecture.** Data preprocessing (grey): Four consecutive input images ($t_{n-1}, \dots, t_{n+2}$) are center cropped. For the *absolute* network the mean is subtracted. For the *relative* network the OF is precomputed by FlowNet2.0 [25]. The *absolute* poses are predicted by our *time-distributed* APR-network (yellow). The RPR-network (purple) predicts the transformed *relative* displacements and rotations on reshaped mean vectors of the OF with (stacked) LSTM-RNNs. The PE modules (green) concatenates the absolute and relative modules and predicts the absolute 6DoF poses with stacked LSTM-RNNs.

is obtained by a back-transformation of the predicted displacement, such that

$$\boldsymbol{R}^T = \boldsymbol{R}^{-1} \quad \text{and} \quad \boldsymbol{R}^T\boldsymbol{R} = \boldsymbol{R}\boldsymbol{R}^T = \boldsymbol{I}. \tag{3}$$

Fig. 4 shows the structure of the RPR-network. Similar to the APR-network, the RPR-network also uses a stack of images, i.e., three OF-fields from the four input images of the timesteps $t_{n-1}, \dots, t_{n+2}$, to include more time context.

In a preliminary study, we found that our recurrent units struggle to remember temporal features when the direct input of the OF is too large (raw size $224 \times 224 \times 3\, px$). This is in line with findings from Walch et al. [77]. Hence, we split the OF in zones and compute the mean value for each the u- and v-direction. We reshape 16×16 number of zones in both directions to the size 2×256. The final concatenation results in a smaller total size of 3×512. The LSTM-output is forwarded to 2 FC-layers that regress both the displacement (size 3×3) and rotation (size 3×4).

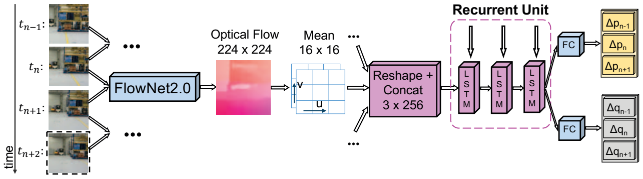

Figure 4: Pipeline of the *relative* pose regression (RPR) architecture: Data preprocessing, OF- and mean computation, reshaping, and concatenation, 3 recurrent LSTM units, and 2 FC-layers that yield the relative pose.

The 2 FC-layers use the following loss function to predict the relative transposed poses $\Delta\tilde{\boldsymbol{p}}^{tr}$ and $\Delta\boldsymbol{q}$:

$$\mathcal{L} = \alpha_2 \left\| \Delta\tilde{\boldsymbol{p}}^{tr} - \Delta\boldsymbol{p}^{tr} \right\|_2 + \beta_2 \left\| \Delta\tilde{\boldsymbol{q}} - \frac{\Delta\boldsymbol{q}}{\|\Delta\boldsymbol{q}\|_2} \right\|_2 . \tag{4}$$

The first term accounts for the predicted and transformed displacement $\Delta\tilde{\boldsymbol{p}}^{tr}$ to the ground truth displacement $\Delta\boldsymbol{p}^{tr}$ with an L^2-norm. The second term quantifies the error of the predicted rotation to the normalized ground truth rotation using an L^2-norm. Both terms are weighted by the hyperparameters α_2 and β_2. A preliminary grid search with a fixed $\alpha_2 = 1$ revealed an optimal value for β_2 that depends on the scaling of the environment.

3.3. 6DoF Pose Estimation (PE) Network

Our PE-network predicts absolute 6DoF poses from the outputs of both the APR- and RPR-networks, see Fig. 5. The PE-network takes as input the absolute position $\boldsymbol{p}_i = (x_i, y_i, z_i)$, the absolute orientation $\boldsymbol{q}_i = (w_i, p_i, q_i, r_i)$, the relative displacement $\Delta\boldsymbol{p}_i = (\Delta x_i, \Delta y_i, \Delta z_i)$, and the rotation change $\Delta\boldsymbol{q}_i = (\Delta w_i, \Delta p_i, \Delta q_i, \Delta r_i)$. As we feed poses from three sequential timesteps t_{n-1}, t_n, and t_{n+1} as input to the model it is implicitly *time-distributed*. The 2 stacked LSTM-layers and the 2 FC-layers return a 3DoF absolute position $\boldsymbol{p} \in \mathbb{R}^3$ and a 3DoF orientation $\boldsymbol{q} \in \mathbb{R}^4$ using the following loss:

$$\mathcal{L}(P, \Delta P) = \alpha_3 \left\| \tilde{\boldsymbol{p}} - \boldsymbol{p} \right\|_2 + \beta_3 \left\| \tilde{\boldsymbol{q}} - \frac{\boldsymbol{q}}{\|\boldsymbol{q}\|_2} \right\|_2 . \tag{5}$$

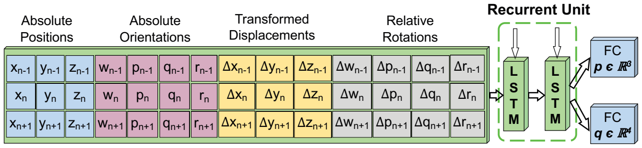
Absolute Positions
Absolute Orientations
Transformed Displacements
Relative Rotations
Recurrent Unit
x_{n-1} y_{n-1} z_{n-1} w_{n-1} p_{n-1} q_{n-1} r_{n-1} Δx_{n-1} Δy_{n-1} Δz_{n-1} Δw_{n-1} Δp_{n-1} Δq_{n-1} Δr_{n-1}
x_n y_n z_n w_n p_n q_n r_n Δx_n Δy_n Δz_n Δw_n Δp_n Δq_n Δr_n
x_{n+1} y_{n+1} z_{n+1} w_{n+1} p_{n+1} q_{n+1} r_{n+1} Δx_{n+1} Δy_{n+1} Δz_{n+1} Δw_{n+1} Δp_{n+1} Δq_{n+1} Δr_{n+1}
LSTM
LSTM
FC $p \in \mathbb{R}^3$
FC $q \in \mathbb{R}^4$

Figure 5: Pipeline of the 6DoF PE-architecture. The input tensor (3×14) contains absolute positions and orientations and relative displacements and rotations at timesteps t_{n-1}, t_n, t_{n+1}. 2 stacked LSTMs process the tensor and 2 FC-layers return the pose.

Again, in a preliminary grid search we chose L_2-norms with a fixed $\beta_3 = 1$ that revealed an optimal value for α_3.

4. Evaluation Datasets

To train our network we need two different types of image data: (1) images annotated with their absolute poses for the APR-network, and (2) images of OF, annotated with their relative poses for the RPR-network.

Datasets to evaluate APR. Publicly available datasets for absolute pose regression (Cambridge Landmarks [33] and TUM-LSI [77]) either lack accurate ground truth labels or the proximity between consecutive images is too large to embed meaningful temporal context. The Aalto University [37], Oxford RobotCar [47], DeepLoc [59] and CMU Seasons [62] datasets solve the small-scale issue of the 7-Scenes [66] dataset, but are barely used for evaluation of state-of-the-art techniques or consider only automotive-driving scenarios. The 12-Scenes [73] dataset is only used by DSAC++ [5]. For our industrial application these datasets are insufficient. 7-Scenes [66] only embeds scenes with less training data and only enables small scene-wise evaluations, but is mainly used for evaluation. Hence, to compare ViPR with recent techniques we use the 7-Scenes [66] dataset. Furthermore, we recorded the *Industry* dataset (see Sec. 4.1) that embeds three different industrial-like scenarios to allow a comprehensive and detailed evaluation with different movement patterns (such as slow motion and fast rotation).

Datasets to evaluate RPR. To evaluate the performance of the RPR and its contribution to ViPR, we also need a dataset with a close proximity between consecutive images. This is key to calculate the relative movement with OF. However, most publicly available datasets (Middlebury [1], MPI Sintel [9], KITTI Vision [21], and FlyingChairs [19]) either do not meet this requirement or the OF pixel velocities do not match those of real-world applications. Hence, we directly calculate the OF from images with FlowNet2.0 [25] to train the RPR on it. Our novel *Industry* dataset allows this, while retaining a large, diverse environment with hard real-world conditions, as described in the following.

4.1. Industry Dataset

We designed the *Industry* dataset to suite the requirements of both the APR- and the RPR-network and published the data[1] at large-scale ($1,320m^2$) using a high-precision ($< 1mm$) laser-based reference system. Each scenario presents different challenges (such as dynamic ego-motion with motion blur), various environmental characteristics (such as different geometric scales, light changes, i.e., artificial and natural light), and ambiguously structured elements, see Fig. 6.

Industry Scenario #1 [44] has been recorded with 8 cameras (approx. 60° field-of-view (FoV) each) mounted on a stable apparatus to cover 360° (with overlaps) that has been moved automatically at a constant velocity of approx. 0.3 m/s. The height of the cameras is at 1.7 m. The scenario contains 521,256 images (640 × 480 px) and densely covers an area of 1,320 m^2. The environment imitates a typical warehouse scenario under realistic conditions. Besides well-structured elements such as high-level racks with goods, there are also very ambiguous and homogeneously textured elements (e.g., blank white or dark black walls). Both natural and artificial light illuminates volatile structures such as mobile work benches. While the training dataset is composed of a horizontal and vertical zig-zag movement of the apparatus the test datasets movements vary to cover different properties for a detailed evaluation, e.g., different environmental scalings (i.e., *scale transition*, *cross*, *large scale*, and *small scale*), network generalization (i.e., *generalize open*, *generalize racks*, and *cross*), fast rotations (i.e., *motion artifacts* was recorded on a forklift at 2.26 m height) and volatile objects (i.e., *volatility*).

Industry Scenario #2 uses three 170° cameras (with overlaps) on the same apparatus at the same height. The recorded 11,859 training images ($1,280 \times 720$ px) represent a horizontal zig-zag movement (see Fig. 7a) and 3,096 test images represent a diagonal movement (see Fig. 7b). Compared to Scenario #1 this scenario has more variation in its velocities (between 0 m/s and 0.3 m/s, SD 0.05 m/s).

Industry Scenario #3 uses four 170° cameras (with overlaps) on a forklift truck at a height of 2.26 m. Both the training and test datasets represents camera movements at varying, faster, and dynamic speeds (between 0 m/s and 1.5 m/s, SD 0.51 m/s). This makes the scenario the most challenging one. The training trajectory (see Fig. 7c) consists of 4,166 images and the test trajectory (see Fig. 7d) consists of 1,687 images. In contrast to the Scenarios #1 and #2 we train and test a typical industry scenario on dynamic movements of a forklift truck. However, one of cameras' images were corrupted in the test dataset, and thus, not used in the evaluation.

[1] *Industry* dataset available at: https://www.iis.fraunhofer.de/warehouse. Provided are **raw images** and corresponding labels: $\boldsymbol{p}$ and $\boldsymbol{q}$.

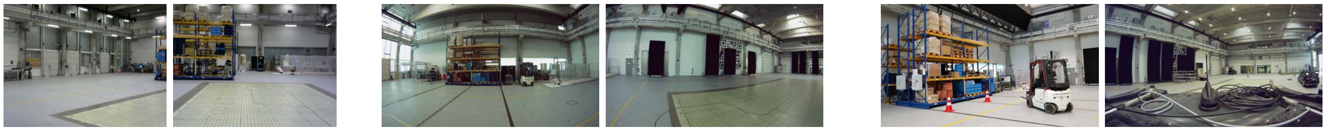

(a) Scenario #1 example images. (b) Scenario #2 example images. (c) Scenario #3 setup and example image.

Figure 6: **Industry datasets.** Setup of the measurement environment (i.e., forklift truck, warehouse racks and black walls) and example images with normal (a) and wide-angle (b+c) cameras.

5. Experimental Results

To compare ViPR with state-of-the-art results, we first briefly describe our parameterization of PoseNet [33] and PoseNet+LSTM [77] in Sec. 5.1. Next, Sec. 5.2 presents our results. We highlight the performance of ViPR's subnetworks (APR, APR+LSTM) individually, and investigate both the impact of RPR and PE on the final pose estimation accuracy of ViPR. Sec. 5.3 shows results of the RPR-network. Finally, we discuss general findings and show runtimes of our models in Sec. 5.4.

For all experiments we used an AMD Ryzen 7 2700 CPU 3.2 *GHz* equipped with one NVidia GeForce RTX 2070 with 8 GB GDDR6 VRAM. Tab. 1 shows the median error of the position in m and the orientation in *degrees*. The second column reports the spatial extends of the datasets. The last column reports the improvement in position accuracy of ViPR (in %) over APR-only.

5.1. Baselines

As a baseline we report the initially described results on 7-Scenes of PoseNet [33] and PoseNet+LSTM [77] (*in italic*). We further re-implemented the initial variant of PoseNet and trained it from scratch with $\alpha_1 = 1, \beta_1 = 30$ (thus optimizing for positional accuracy at the expense of orientation accuracy). Tab. 1 (cols. 3 and 4) shows our implementation's results next to the initially reported ones (on 7-Scenes). We see that (as expected) the results of the PoseNet implementations differ due to changed values for α_1 and β_1 in our implementation.

5.2. Evaluation of the ViPR-Network

In the following, we evaluate our method in multiple scenarios with different distinct challenges for the pose estimation task. 7-Scenes focuses on difficult motion blur conditions of typical human motion. We then use the *Industry Scenario #1* to investigate various challenges at a larger scale, but with mostly constant velocities. *Industry Scenarios #2* and *#3* then focus on dynamic, fast ego-motion of a moving forklift truck at large-scale.

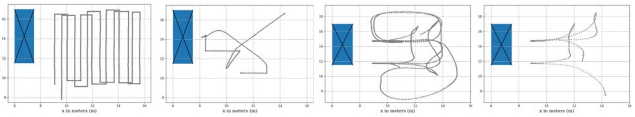

(a) Training. (b) Testing. (c) Training. (d) Testing.

Figure 7: Exemplary trajectories of *Industry Scenarios #2* (a-b) and *#3* (c-d) to assess the generalizability of ViPR.

7-Scenes [66]. For both architectures (PoseNet and ViPR), we optimized β to weight the impact of position and orientation such that it yields the smallest total median error. Both APR+LSTM and ViPR return a slightly lower pose estimation error of 0.33 m and 0.32 m than PoseNet+LSTM with 0.34 m. ViPR yields an average improvement of the position accuracy of 3.18 % even in strong motion blur situations. The results indicate that ViPR relies on a plausible optical flow component to achieve performance that is superior to the baseline. In situations of negligible motion between frames the median only improves by 0.02 m. However, the average accuracy gain still shows that ViPR performs *en par* or better than the baselines.

Stable motion evaluation. For the *Industry Scenario #1* dataset, we train the models on the zig-zag trajectories, and test them on specific sub-trajectories with individual challenges, but at almost constant velocity. In total, ViPR improves the position accuracy by 12.27% on average (min.: 4.03 %; max.: 25.31 %) while the orientation error is similar for most of the architectures and test sets.

In environments with volatile features, i.e., objects that are only present in the test dataset, we found that ViPR (with optical flow) is significantly (6.41 %) better compared to APR-only. However, the high angular error of 77.54° indicates an irrecoverable degeneration of the APR-part. In tests with different scaling of the environment, we think that ViPR learns an interpretation of relative and absolute position regression, that works both in small and large proximity to environmental features, as ViPR improves by 15.52 % (scale trans.) and 14.41 % (small scale) or 10.68 % (large scale). When the test trajectories are located within areas that embed only few or no training samples (gener. racks and open), ViPR still improves over other methods with 4.03-11.75 %. The highly dynamic test on a forklift truck (motion artifacts) is exceptional here as only the test dataset contains dynamics and blur, and hence, challenges ViPR most. However, ViPR still improves by 10.01 % over APR-only, despite the data dynamic's absolute novelty.

In summary, ViPR decreases the position median significantly by about 2.53 m than only APR+LSTM (4.89 m). This and the other findings are strong indicators that the relative component RPR significantly supports the final pose estimation of ViPR.

Table 1: Pose estimation results (position and orientation median error in meters m and degrees ($^\circ$)) and total improvement of PE in $\%$ on the `7-Scenes` [66] and *Industry* datasets. The best results are bold and underlined ones are additionally referenced in the text.

	Dataset	Spatial extend (m)	PoseNet [33] (*original*/our param.)		PoseNet+ LSTM [77]		APR-only		APR+LSTM (our param.)		ViPR*		Improv. ViPR (%)
`7-Scenes` [66]	chess	3.0 × 2.0 × 1.0	*0.32* / 0.24	*4.06* / 7.79	*0.24*	*5.77*	0.23	7.96	0.27	9.66	**0.22**	**7.89**	+ 1.74
	fire	2.5 × 1.0 × 1.0	*0.47* / 0.39	*14.4* / 12.40	*0.34*	*11.9*	0.39	12.85	0.50	15.70	**0.38**	**12.74**	+ 2.56
	heads	2.0 × 0.5 × 1.0	*0.29* / 0.21	*6.00* / 16.46	*0.21*	*13.7*	0.22	16.48	0.23	16.91	**0.21**	**16.41**	+ 3.64
	office	2.5 × 2.0 × 1.5	*0.48* / 0.33	*3.84* / 10.08	*0.30*	*8.08*	0.36	10.11	0.37	10.83	**0.35**	**9.59**	+ 4.01
	pumpkin	2.5 × 1.0 × 1.0	*0.47* / 0.45	*8.42* / 8.70	*0.33*	*7.00*	0.39	8.57	0.86	49.46	**0.37**	**8.45**	+ 5.12
	red kitchen	4.0 × 3.0 × 1.5	*0.59* / 0.41	*8.64* / 9.08	*0.37*	*8.83*	0.42	9.33	1.06	50.67	**0.40**	**9.32**	+ 4.76
	stairs	2.5 × 2.0 × 1.5	*0.47* / 0.36	*6.93* / 13.69	*0.40*	*13.7*	0.31	12.49	0.42	13.50	**0.31**	12.65	+ 0.46
	∅ total		*0.44* / 0.34	*7.47* / 11.17	*0.31*	*9.85*	0.33	11.11	0.53	23.82	**0.32**	**11.01**	**+ 3.18**
Industry *Scenario 1* [44]	cross	24.5 × 16.0	– / 1.15	– / 0.75	–		0.61	0.53	4.42	0.21	**0.46**	0.60	+ 25.31
	gener. open	20.0 × 17.0	– / 1.94	– / 11.73	–		1.68	11.07	3.36	2.95	**1.48**	**10.86**	+ 11.75
	gener. racks	8.5 × 18.5	– / 3.48	– / 6.01	–		2.48	1.53	3.90	0.61	**2.38**	1.95	+ 4.03
	large scale	19.0 × 19.0	– / 2.32	– / 6.37	–		2.37	9.82	4.99	1.61	**2.12**	8.64	+ 10.68
	motion art.	37.0 × 17.0	– / 7.43	– / 124.94	–		7.48	131.30	8.18	139.37	**6.73**	136.6	+ 10.01
	scale trans.	28.0 × 19.5	– / 2.17	– / 3.03	–		1.94	6.46	5.63	0.58	**1.64**	6.29	+ 15.52
	small scale	10.0 × 11.0	– / 3.78	– / 9.18	–		4.09	20.75	4.46	6.06	**3.50**	15.74	+ 14.41
	volatility	29.0 × 13.0	– / 2.68	– / 78.52	–		2.09	77.68	4.16	78.73	**1.96**	77.54	+ 6.41
	∅ total		– / 3.12	– / 30.07	–		2.82	32.30	4.89	28.76	**2.53**	32.28	**+ 12.27**
Industry *Scen. 2*	cam #0	6.5 × 9.0	– / 0.49	– / 0.21	–		0.22	0.29	1.49	0.14	**0.16**	3.37	+ 26.24
	cam #1	6.5 × 9.0	– / 0.15	– / 0.38	–		0.23	0.35	2.68	0.17	**0.12**	2.75	+ 46.49
	cam #2	6.5 × 9.0	– / 0.43	– / 0.19	–		0.37	0.13	0.90	0.15	**0.30**	1.84	+ 17.87
	∅ total		– / 0.36	– / 0.26	–		0.27	0.26	1.69	0.15	**0.20**	2.65	**+ 30.20**
Industry *Scen. 3*	cam #0	6.0 × 11.0	– / 0.41	– / 1.00	–		0.34	1.26	0.72	1.31	**0.27**	1.43	+ 20.64
	cam #1	6.0 × 11.0	– / 0.32	– / 1.07	–		0.26	1.11	0.88	1.27	**0.21**	**1.06**	+ 20.13
	cam #2	6.0 × 11.0	– / 0.32	– / 1.60	–		0.36	1.62	0.72	1.74	**0.32**	**1.38**	+ 11.47
	∅ total		– / 0.35	– / 1.22	–		0.32	1.33	0.77	1.44	**0.27**	1.29	**+ 17.41**

Industry Scenario #2 is designed to evaluate for unknown trajectories. Hence, training trajectories represent an orthogonal grid, and test trajectories are diagonal. In total, ViPR improves the position accuracy by $30.2\,\%$ on average (min.: $17.87\,\%$; max.: $46.49\,\%$). Surprisingly, the orientation error is comparable for all architectures, except ViPR. We think that this is because ViPR learns to optimize its position based on the APR- and RPR- orientations, and hence, exploits these orientations to improve its position estimate, that we prioritized in the loss function. APR-only yields an average position accuracy of $0.27\,m$, while the pure `PoseNet` yields position errors of $0.36\,m$ on average, but APR+LSTM results in an even worse accuracy of $1.69\,m$. Instead, the novel ViPR outperforms all significantly with $0.2\,m$. Compared to our APR+LSTM approach, we think that ViPR on the one hand interprets and compensates the (long-term) drift of RPR and on the other hand smooths the short-term errors of APR, as PE counteracts the accumulation of RPR's scaling errors with APR's absolute estimates. Here, the synergies of the networks in ViPR are particularly effective. This is also visualized in Fig. 8a: the green (ViPR) trajectory aligns more smoothly to the blue baseline when the movement direction changes. This also indicates that the RPR component is necessary to generalize to unknown trajectories and to compensate scaling errors.

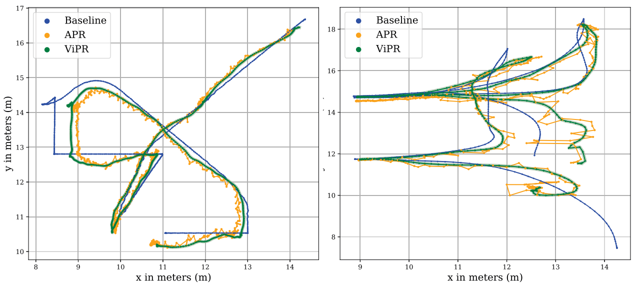

(a) *Scenario #2*.

(b) *Scenario #3*.

Figure 8: Exemplary comparison of APR, ViPR, and a baseline (ground truth) trajectory of the *Industry* datasets.

Dynamic motion evaluation. In contrast to the other datasets, the *Industry Scenario #3* includes fast, large-scale, and high dynamic ego-motion in both training and test datasets. However, all estimators result in similar findings as *Scenario #2* as both scenarios embed motion dynamics and unknown trajectory shapes. Accordingly, ViPR again improves the position accuracy by $17.41\,\%$ on average (min.: $11.47\,\%$; max.: $20.64\,\%$), but this time exhibits very similar orientation errors. Improved orientation accuracy compared to *Scenario #2* is likely due to diverse orientations available in this dataset's training.

Fig. 8b shows exemplary results that visualize how ViPR handles especially motion changes and motion dynamics (see the abrupt direction change between $x \in [8-9]\,m$ and $y \in [14-16]\,m$). The results also indicate that ViPR predicts the smoothest and most accurate trajectories on unknown trajectory shapes (compare the trajectory segments between $x \in [11-12]\,m$ and $y \in [14-16]\,m$). We think the reason why ViPR significantly outperforms APR

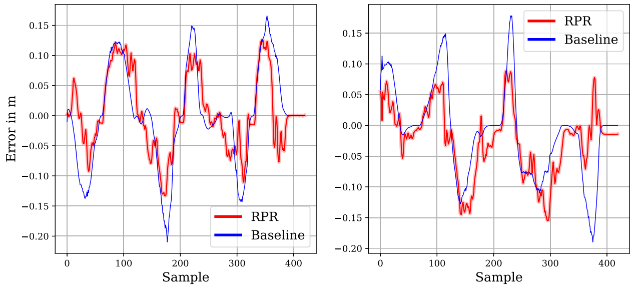

Figure 9: Exemplary RPR-results (displacements m) against the baseline (ground truth) on the *Scenario #3* dataset (see Fig. 7d).

by 20.13 % here is because of the synergy of APR, RPR, and PE. RPR contributes most in fast motion-changes, i.e., in motion blur situation. The success of RPR may also indicate that RPR differentiates between ego- and feature-motion to more robustly estimate a pose.

5.3. Evaluation of the RPR-Network

We use the smaller FlowNet2-s [25] variant of `FlowNet2.0` as this has faster runtimes (140 *Hz*), and use it pretrained on the FlyingChairs [19], ChairsSDHom and FlyingThings3D datasets. To highlight that RPR contributes to the accuracy of the final pose estimates of ViPR, we explicitly test it on the *Industry Scenario #3* that embeds dynamic motion of both ego- and feature-motion. The distance between consecutive images is up to 20 cm, see Fig. 9. This results in a median error of 2.49 cm in x- and 4.09 cm in y-direction on average (i.e., the error is between 12.5 % and 20.5 %). This shows that the RPR yields meaningful results for relative position regression in a highly dynamic and difficult setting. It furthermore appears to be relatively robust in its predictions despite both ego- and feature-motion.

5.4. Discussion

6DoF Pose Regression with LSTMs. APR-only increases the positional accuracy over `PoseNet` for all datasets, see Tab. 1. We found that the position errors increase when we use methods with independent and single-layer LSTM-extensions [77, 79, 58, 65] on both the `7-Scenes` and the *Industry* datasets, by 0.04 m up to 2.07 m. This motivated us to investigate stacked LSTM-layers only for the RPR- and PE-networks. We support the statement of Seifi et al. [65] that the motion between consecutive frames is too small, and thus, naive CNNs are already unable to embed them. Hence, additionally connected LSTMs are also unable to discover and track meaningful temporal and contextual relations between the features.

Influence of RPR to ViPR. To figure out the information gain of the RPR-network we also constructed ViPR in a closed end-to-end architecture through direct concatenation of the CNN-encoder-output (APR) and the LSTM-output (RPR). For a smaller OF-input (3 × 3) of the RPR-model the accuracy of the `7-Scenes` [66] dataset increases, but decreases for the *Industry* dataset. This stems from the fact that the relative movements of the `7-Scenes` dataset are too small ($< 2\,cm$) compared to the *Industry* dataset (approx. 20 cm). Hence, ViPR's contribution is limited here.

Comparison of ViPR to state-of-the-art methods. `VLocNet++` [59] currently achieves the best results on `7-Scenes` [66], but due to the small relative movement and the high ground truth error compared to `VLocNet`'s results a plausible evaluation is not possible regarding industrial applications. `MapNet` [8] achieves (on average) better results than ViPR on the `7-Scenes` dataset, but results in a similar error, e.g., 0.30 m and 12.08° on the *stairs* set against ViPR's 0.31 m and 12.65°. `MapNet` has an improvement of 8.7 % over `PoseNet2` [32] and achieves 41.4 m and 12.5 ° on the `RobotCar` [47] dataset. However, a fair evaluation on this dataset with state-of-the-art methods requires results and code from `VLocNet` [72, 59].

Runtimes. The training of the APR takes 0.86 s per iteration for a batch size of 50 (GoogLeNet [68]) on our hardware setup. The training of the RPR and PE is faster (0.065 s) even at a higher batch size of 100, as these models are smaller (214,605, resp. 55,239, parameters). Hence, it is possible to retrain the PE-network quickly upon environment changes. The inference time of ViPR is between 7 *ms* and 9 *ms* per sample (`PoseNet`: avg. 5 *ms*, `FlowNet2-s`: avg. 9 *ms*). In addition, ViPR does not require domain knowledge to provide scenario-dependent applicability, nor does it need a compute-intensive matcher like brute force or `RANSAC` [67, 6]. However, instead of `PoseNet`, ViPR can also use such classical approaches in its modular process pipeline. `DenseVLAD` [71] and classical approaches are 10x (200-350 *ms*/sample) more computationally intensive than today's deep pose regression variants.

6. Conclusion

In this paper, we addressed typical challenges of learning-based visual self-localization of a monocular camera. We introduced a novel DL-architecture that makes use of three modules: an absolute and a relative pose regressor module, and a final regressor that predicts a 6DoF pose by concatenating the predictions of the two former modularities. To show that our novel architecture improves the absolute pose estimates, we compared it with a publicly available dataset and proposed novel *Industry* datasets that enable a more detailed evaluation of different (dynamic) movement patterns, generalization, and scale transitions.

Acknowledgements

This work was supported by the Bavarian Ministry for Economic Affairs, Infrastructure, Transport and Technology through the Center for Analytics-Data-Applications (ADA-Center) within the framework of "BAYERN DIGI-TAL II".

References

[1] Simon Baker, Stefan Roth, Daniel Scharstein, Michael J. Black, J. P. Lewis, and Richard Szeliski. "A Database and Evaluation Methodology for Optical Flow". In *Intl. Conf. on Computer Vision (ICCV)*, pages 1–8, Rio de Janeiro, Brazil, 2007. 3, 5

[2] Vassileios Balntas, Shuda Li, and Victor Prisacariu. "RelocNet: Continuous Metric Learning Relocalisation Using Neural Nets". In *Europ. Conf. on Computer Vision (ECCV)*, 2018. 2

[3] Alessandro Bergamo, Sudipta N. Sinha, and Lorenzo Torresani. "Leveraging Structure from Motion to Learn Discriminative Codebooks for Scalable Landmark Classification". In *Intl. Conf. on Computer Vision and Pattern Recognition (CVPR)*, pages 763–770, Portland, OR, 2013. 2

[4] James Bergen. Visual odometry. *Intl. Journal of Robotics Research*, 33(7):8–18, 2004. 2

[5] Eric Brachman and nCarsten Rother. "Expert Sample Consensus Applied to Camera Re-Localization". In *Intl. Conf. on Computer Vision (ICCV)*, Oct. 2019. 5

[6] Eric Brachmann, Alexander Krull, Sebastian Nowozin, Jamie Shotton, Frank Michel Stefan Gumhold, and Carsten Rother. "DSAC — Differentiable RANSAC for Camera Localization". In *Intl. Conf. on Computer Vision and Pattern Recognition (CVPR)*, pages 2492–2500, Honolulu, HI, 2017. 1, 2, 8

[7] Eric Brachmann, Frank Michel, Alexander Krull, Michael Ying Yang, Stefan Gumhold, and Carsten Rother. "Uncertainty-Driven 6D Pose Estimation of Objects and Scenes from a Single RGB Image". In *Intl. Conf. on Computer Vision and Pattern Recognition (CVPR)*, pages 3364–3372, Las Vegas, NV, 2016. 1

[8] Samarth Brahmbhatt, Jinwei Gu, Kihwan Kim, James Hays, and Jan Kautz. "Geometry-Aware Learning of Maps for Camera Localization". In *Intl. Conf. on Computer Vision and Pattern Recognition (CVPR)*, pages 2616–2625, Salt Lake City, UT, 2018. 3, 8

[9] Daniel J. Butler, Jonas Wulff, Garrett B. Stanley, and MichaelJ. Black. "A Naturalistic Open Source Movie for Optical Flow Evaluation". In *Proc. Europ. Conf. on Computer Vision (ECCV)*, pages 611–625, Florence, Italy, 2012. 5

[10] Cesar Cadena, Luca Carlone, Henry Carrillo, Yasir Latif, Davide Scaramuzza, José Neira, Ian Reid, and John J Leonard. Past, present, and future of simultaneous localization and mapping: Toward the robust-perception age. *Trans. on Robotics*, 32(6):1309–1332, 2016. 2

[11] Ming Chi, Chunhua Shen, and Ian Reid. "A Hybrid Probabilistic Model for Camera Relocalization". In *British Machine Vision Conf. (BMVC)*, York, UK, 2018. 1

[12] Ronald Clark, Sen Wang, Andrew Markham, Niki Trigoni, and Hongkai Wen. "VidLoc: A Deep Spatio-Temporal Model for 6-DoF Video-Clip Relocalization". In *Conf. on Computer Vision and Pattern Recognition (CVPR)*, pages 2652–2660, Honolulu, HI, 2017. 3

[13] Gabriele Costante and Thomas Alessandro Ciarfuglia. "LS-VO: Learning Dense Optical Subspace for Robust Visual Odometry Estimation". In *Robotics and Automation Letters*, volume 3, pages 1735–1742, July 2018. 3

[14] Gabriele Costante, Michele Mancini, Paolo Valigi, and Thomas A. Ciarfuglia. "Exploring Representation Learning With CNNs for Frame-to-Frame Ego-Motion Estimation". In *Robotics and Automation Letters*, volume 1, Jan. 2016. 3

[15] Mingyu Ding, Zhe Wang, Jiankai Sun, Jianping Shi, and Ping Luo. "CamNet: Coarse-to-Fine Retrieval for Camera Re-Localization". In *Intl. Conf. on Computer Vision (ICCV)*, pages 2871–2880, Seoul, South Korea, 2019. 2

[16] Nam-Duong Duong, Amine Kacete, Catherine Sodalie, Pierre-Yves Richard, and Jérôme Royan. "xyzNet: Towards Machine Learning Camera Relocalization by Using a Scene Coordinate Prediction Network". In *Intl. Symposium on Mixed and Augmented Reality Adjunct (ISMAR-Adjunct)*, pages 258–263, Munich, Germany, 2018. 1

[17] Ryan C. DuToit, Joel A. Hesch, Esha D. Nerurkar, and Stergios I. Roumeliotis. "Consistent map-based 3D localization on mobile devices". In *Intl. Conf. on Robotics and Automation (ICRA)*, pages 6253–6260, Singapore, Singapore, 2017. 2

[18] Tobias Feigl, Andreas Porada, Steve Steiner, Christoffer Löffler, Christopher Mutschler, and Michael Philippsen. "Localization Limitations of ARCore, ARKit, and Hololens in Dynamic Large-Scale Industry Environments". In *Intl. Conf. on Computer Graphics Theory and Applications*, Jan. 2020. 2

[19] Philipp Fischer, Alexey Dosovitskiy, Eddy Ilg, Philipp Häusser, Caner Hazirbas, Vladimir Golkov, Patrick van der Smagt, Daniel Cremers, and Thomas Brox. "FlowNet: Learning Optical Flow with Convolutional Networks". In *Intl. Conf. on Computer Vision (ICCV)*, pages 2758–2766, Santiago de Chile, Chile, 2015. 5, 8

[20] Yarin Gal and Zoubin Ghahramani. "Bayesian Convolutional Neural Networks with Bernoulli Approximate Variational Inference". In *arXiv preprint arXiv:1506.02158*, 2016. 2

[21] Andreas Geiger, Philip Lenz, and Raquel Urtasun. "Are we ready for autonomous driving? The Kitti vision benchmark suite". In *Intl. Conf. on Computer Vision and Pattern Recognition (CVPR)*, pages 3354–3361, Providence, RI, 2012. 5

[22] Marcel Geppert, Peidong Liu, Zhaopeng Cui, Marc Pollefeys, and Torsten Sattler. "Efficient 2D-3D Matching for Multi-Camera Visual Localization". In *Intl. Conf. on Robotics and Automation (ICRA)*, pages 5972–5978, Montreal, Canada, 2019. 2

[23] Abner Guzman-Rivera, Pushmeet Kohli, Ben Glocker, Jamie Shotton, Toby Sharp, Andrew Fitzgibbon, and Shahram Izadi. "Multi-output Learning for Camera Relocalization". In *Intl. Conf. on Computer Vision and Pattern Recognition (CVPR)*, pages 1114–1121, Columbus, OH, 2014. 1

[24] Qiang Hao, Rui Cai, Zhiwei Li, Lei Zhang, Yanwei Pang, and Feng Wu. "3D visual phrases for landmark recognition". In *Intl. Conf. on Computer Vision and Pattern Recognition (CVPR)*, pages 3594–3601, Providence, RI, 2012. 2

[25] Eddy Ilg, Nikolaus Mayer, Tonmoy Saikia, Margret Keuper, Alexey Dosovitskiy, and Thomas Brox. "FlowNet 2.0: Evolution of Optical Flow Estimation with Deep Networks". In *Intl. Conf. on Computer Vision and Pattern Recognition (CVPR)*, pages 1647–1655, Honolulu, HI, 2017. 2, 3, 4, 5, 8

[26] Ganesh Iyer, J. Krishna Murthy, Gunshi Gupta, K. Madhava Krishna, and Liam Paull. "Geometric Consistency for Self-Supervised End-to-End Visual Odometry". In *Intl. Conf. on Computer Vision and Pattern Recognition (CVPR) Workshops*, Salt Lake City, UT, 2018. 1

[27] Gijeong Jang, Sungho Lee, and Inso Kweon. "Color landmark based self-localization for indoor mobile robots". In *Intl. Conf. on Robotics and Automation (ICRA)*, pages 1037–1042, Washington, DC, 2002. 1

[28] Eagle S. Jones and Stefano Soatto. "Visual-Inertial Navigation, Mapping and Localization: A Scalable Real-Time Causal Approach". In *Intl. Journal of Robotics Research*, volume 30, pages 407–430, 2011. 2

[29] Anton Kasyanov, Francis Engelmann, Jörg Stückler, and Bastian Leibe. Keyframe-based visual-inertial online slam with relocalization. In *Proc. Intl. Conf. on Intelligent Robots and Systems (IROS)*, pages 6662–6669, Vancouver, Canada, 2017. 2

[30] H. Kato and M. Billinghurst. Marker tracking and HMD calibration for a video-based augmented reality conferencing system. In *Proc. Intl. Workshop on Augmented Reality (IWAR)*, pages 85–94, San Francisco, CA, 1999. 2

[31] Alex Kendall and Roberto Cipolla. "Modelling Uncertainty in Deep Learning for Camera Relocalization". In *Intl. Conf. on Robotics and Automation (ICRA)*, pages 4762–4769, Stockholm, Sweden, 2016. 1, 2

[32] Alex Kendall and Roberto Cipolla. "Geometric Loss Functions for Camera Pose Regression with Deep Learning". In *Intl. Conf. on Computer Vision and Pattern Recognition (CVPR)*, pages 6555–6564, Honolulu, HI, 2017. 2, 3, 8

[33] Alex Kendall, Matthew Grimes, and Roberto Cipolla. "PoseNet: A Convolutional Network for Real-Time 6-DOF Camera Relocalization". In *Intl. Conf. on Computer Vision (ICCV)*, pages 2938–2946, Santiago de Chile, Chile, 2015. 1, 2, 3, 5, 6, 7

[34] Christian Kerl, Jurgen Sturm, and Daniel Cremers. Dense visual SLAM for RGB-d cameras. In *Proc. Intl. Conf. on Intelligent Robots and Systems (IROS)*, pages 2100–2106, Tokyo, Japan, 2013. 2

[35] Georg Klein and David Murray. Parallel tracking and mapping for small AR workspaces. In *Proc. Intl. Workshop on Augmented Reality (ISMAR)*, pages 1–10, Nara, Japan, 2007. 2

[36] Robin Kreuzig, Matthias Ochs, and Rudolf Mester. "DistanceNet: Estimating Traveled Distance From Monocular Images Using a Recurrent Convolutional Neural Network". In *Intl. Conf. on Computer Vision and Pattern Recognition (CVPR) Workshops*, Long Beach, CA, 2019. 1

[37] Zakaria Laskar, Iaroslav Melekhov, Surya Kalia, and Juho Kannala. "Camera Relocalization by Computing Pairwise Relative Poses Using Convolutional Neural Network". In *Intl. Conf. on Computer Vision Workshop (ICCVW)*, pages 920–929, Venice, Italy, 2017. 2, 5

[38] Sooyong Lee and Jae-Bok Song. "Mobile robot localization using infrared light reflecting landmarks". In *Intl. Conf. Control, Automation and Systems*, pages 674–677, Seoul, South Korea, 2007. 1

[39] Peiliang Li, Tong Qin, Botao Hu, Fengyuan Zhu, and Shaojie Shen. Monocular visual-inertial state estimation for mobile augmented reality. In *Proc. Intl. Conf. on Intelligent Robots and Systems (IROS)*, pages 11–21, Vancouver, Canada, 2017. 2

[40] Wenbin Li, Sajad Saeedi, John McCormac, Ronald Clark, Dimos Tzoumanikas, Qing Ye, Yuzhong Huang, Rui Tang, and Stefan Leutenegger. Interiornet: Mega-scale multi-sensor photo-realistic indoor scenes dataset. *arXiv preprint arXiv:1809.00716*, 18(17), 2018. 2

[41] Yunpeng Li, Noah, Noah Snavely, Dan Huttenlocher, and Pascal Fua. "Worldwide Pose Estimation Using 3D Point Clouds". In *Europ. Conf. on Computer Vision (ECCV)*, Oct. 2012. 2

[42] Yimin Lin, Zhaoxiang Liu, Jianfeng Huang, Chaopeng Wang, Guoguang Du, Jinqiang Bai, Shiguo Lian, and Bill Huang. "Deep Global-Relative Networks for End-to-End 6-DoF Visual Localization and Odometry". In *Pacific Rim Intl. Conf. Artificial Intelligence (PRICAI)*, pages 454–467, Yanuca Island, Cuvu, Fiji, 2019. 1, 3

[43] Haomin Liu, Mingyu Chen, Guofeng Zhang, Hujun Bao, and Yingze Bao. Ice-ba: Incremental, consistent and efficient bundle adjustment for visual-inertial slam. In *Intl. Conf. on Computer Vision and Pattern Recognition (CVPR)*, pages 1974–1982, Salt Lake City, Utah, 2018. 2

[44] Christoffer Löffler, Sascha Riechel, Janina Fischer, and Christopher Mutschler. "Evaluation Criteria for Inside-Out Indoor Positioning Systems Based on Machine Learning". In *Intl. Conf. on Indoor Positioning and Indoor Navigation (IPIN)*, pages 1–8, Nantes, France, Sept. 2018. 1, 5, 7

[45] David G. Lowe. "Distinctive Image Features from Scale-Invariant Keypoints". In *Intl. Journal of Computer Vision*, volume 60(2), pages 91—-110, 2004. 2

[46] Simon Lynen, Torsten Sattler, Michael Bosse, Joel A. Hesch, Marc Pollefeys, and Roland Siegwart. "Get Out of My Lab: Large-scale, Real-Time Visual-Inertial Localization". In *Robotics: Science ans Systems*, 2015. 2

[47] Will Maddern, Geoffrey Pascoe, Chris Linegar, and Paul Newman. "1 Year, 1000km: The Oxford RobotCar Dataset". In *Intl. Journal of Robotics Research (IJRR)*, pages 3–15, 2016. 5, 8

[48] Syaiful Mansur, Muhammad Habib, Gilang Nugraha Putu Pratama, Adha Imam Cahyadi, and Igi Ardiyanto. Real Time Monocular Visual Odometry using Optical Flow: Study on Navigation of Quadrotora's UAV. In *Intl. Conf. on Science and Technology - Computer (ICST)*, pages 122–126, Yogyakarta, Indonesia, 2017. 3

[49] Eric Marchand, Hideaki Uchiyama, and Fabien Spindler. Pose estimation for augmented reality: A hands-on survey. *Trans. Visualization and Computer Graphics*, 22(12):2633–2651, 2016. 2

[50] Iaroslav Melekhov, Juha Ylioinas, Juho Kannala, and Esa Rahtu. "Image-Based Localization Using Hourglass Networks". In *Intl. Conf. on Computer Vision Workshop (ICCVW)*, pages 870–877, Venice, Italy, 2017. 1

[51] Lili Meng, Jianhui Chen, Frederick Tung, James J. Little, Julien Valentin, and Clarence W. da Silva. "Backtracking

Regression Forests for Accurate Camera Relocalization". In *Proc. Intl. Conf. on Intelligent Robots and Systems (IROS)*, pages 6886–6893, Vancouver, BC, 2017. 1

[52] Sven Middelberg, Torsten Sattler, Ole Untzelmann, and Leif Kobbelt. "Scalable 6-DOF Localization on Mobile Devices". In *Europ. Conf. on Computer Vision (ECCV)*, 2014. 2

[53] Peter Muller and Andreas Savakis. "Flowdometry: An Optical Flow and Deep Learning Based Approach to Visual Odometry". In *Winter Conf. on Applications of Computer Vision (WACV)*, pages 624–631, Santa Rosa, CA, 2017. 3

[54] Raul Mur-Artal and Juan D. Tardos. ORB-SLAM2: An open-source SLAM system for monocular, stereo, and RGB-d cameras. *Trans. Robotics*, 33(5):1255–1262, 2017. 2

[55] Raúl Mur-Artal and Juan D. Tardós. "Visual-Inertial Monocular SLAM With Map Reuse". In *Robotics and Automation Letters*, volume 2, pages 796–803, Apr. 2017. 2

[56] Tayyab Naseer and Wolfram Burgard. "Deep Regression for Monocular Camera-based DoF Global Localization in Outdoor Environments". In *Proc. Intl. Conf. on Intelligent Robots and Systems (IROS)*, pages 1525–1530, Vancouver, BC, 2017. 2

[57] Riccardo Palmarini, John Ahmet Erkoyuncu, and Rajkumar Roy. An innovative process to select augmented reality (AR) technology for maintenance. In *Proc. Intl. Conf. on Manufacturing Systems (CIRP)*, volume 59, pages 23–28, Taichung, Taiwan, 2017. 2

[58] Mitesh Patel, Brendan Emery, and Yan-Ying Chen. "ContextualNet: Exploiting Contextual Information using LSTMs to Improve Image-based Localization". In *Intl. Conf. Robotics and Automation (ICRA)*, 2018. 2, 3, 8

[59] Noha Radwan, Abhinav Valada, and Wolfram Burgard. "VLocNet++: Deep Multitask Learning for Semantic Visual Localization and Odometry". *Robotics and Automation Letters*, 3(4):4407–4414, 2018. 1, 3, 5, 8

[60] Soham Saha, Girish Varma, and C.V.Jawahar. "Improved Visual Relocalization by Discovering Anchor Points". In *arXiv preprint arXiv:1811.04370*, Nov. 2018. 2

[61] Torsten Sattler, Bastian Leibe, and Leif Kobbelt. "Efficient & Effective Prioritized Matching for Large-Scale Image-Based Localization". In *Trans. on Pattern Analysis and Machine Intelligence (TPAM)*, volume 39(9), pages 1744–1756, Sept. 2017. 2

[62] Torsten Sattler, Will Maddern, Carl Toft, Akihiko Torii, Lars Hammarstrand, Erik Stenborg, Daniel Safari, Masatoshi Okutomi, Marc Pollefeys, Josef Sivic, Fredrik Kahl, and Tomas Pajdla. "Benchmarking 6DOF Outdoor Visual Localization in Changing Conditions". In *Intl. COnf. on Computer Vision and Pattern Recognition (CVPR)*, June 2018. 5

[63] Torsten Sattler, Qunjie Zhou, Marc Pollefeys, and Laura Leal-Taixé. "Understanding the Limitations of CNN-based Absolute Camera Pose Regression". In *Intl. Conf. on Computer Vision and Pattern Recognition (CVPR)*, pages 3302–3312, Long Beach, CA, 2019. 1, 2

[64] Thomas Schneider, Marcin Dymczyk, Marius Fehr, Kevin Egger, Simon Lynen, Igor Gilitschenskiz, and Roland Siegwart. "maplab: An Open Framework for Research in Visual-inertial Mapping and Localization". In *Robotics and Automation Letters*, volume 3, pages 1418–1425, July 2018. 2

[65] Soroush Seifi and Tinne Tuytelaars. "How to improve CNN-based 6-DoF Camera Pose Estimation". In *Intl. Conf. on Computer Vision (ICCV)*, 2019. 2, 3, 8

[66] Jamie Shotton, Ben Glocker, Christopher Zach, Shahram Izadi, Antonio Criminisi, and Andrew Fitzgibbon. "Scene Coordinate Regression Forests for Camera Relocalization in RGB-D Images". In *Intl. Conf. on Computer Vision and Pattern Recognition (CVPR)*, pages 2930–2937, Portland, OR, 2013. 1, 2, 5, 6, 7, 8

[67] Chris Sweeney, Victor Fragoso, Tobias H. Höllerer, Matthew Tur, and kMatthew Turk. "Large Scale SfM with the Distributed Camera Model". In *arXiv preprint arXiv:1607.03949*, July 2016. 2, 8

[68] Christian Szegedy, Wei Liu, Yangqing Jia, Pierre Sermanet, Scott Reed, Dragomir Anguelov, Dumitru Erhan, Vincent Vanhoucke, and Andrew Rabinovich. "Going deeper with convolutions". In *Intl. Conf. on Computer Vision and Pattern Recognition (CVPR)*, pages 1–9, Boston, MA, 2015. 3, 8

[69] Takafumi Taketomi, Hideaki Uchiyama, and Sei Ikeda. Visual SLAM algorithms: a survey from 2010 to 2016. *Trans. Computer Vision and Applications*, 9(1):452–461, 2017. 2

[70] Takahiro Terashima and Osamu Hasegawa. A visual-SLAM for first person vision and mobile robots. In *Proc. Intl. Conf. on Intelligent Robots and Systems (IROS)*, pages 73–76, Vancouver, Canada, 2017. 2

[71] Akihiko Torii, Relja Arandjelović, Josef Sivic, Masatoshi Okutomi, and Tomas Pajdla. "24/7 place recognition by view synthesis". In *Intl. Conf. on Computer Vision and Pattern Recognition (CVPR)*, pages 1808–1817, Boston, MA, 2015. 2, 8

[72] Abhinav Valada, Noha Radwan, and Wolfram Burgard. "Deep Auxiliary Learning for Visual Localization and Odometry". In *Intl. Conf. on Robotics and Automation (ICRA)*, pages 6939–6946, Brisbane, Australia, 2018. 1, 3, 8

[73] Julien Valentin, Angela Dai, Matthias Niessner, Pushmeet Kohli, Philip Torr, Shahram Izadi, and Cem Keskin. "Learning to Navigate the Energy Landscape". In *Intl. Conf. on 3D Vision (3DV)*, Oct. 2016. 5

[74] Julien Valentin, Matthias Nießner, Jamie Shotton, Andrew Fitzgibbon, Shahram Izadi, and Philip Torr. "Exploiting uncertainty in regression forests for accurate camera relocalization". In *Intl. Conf. on Computer Vision and Pattern Recognition (CVPR)*, pages 4400–4408, Boston, MA, 2015. 1

[75] Reid Vassallo, Adam Rankin, Elvis C. S. Chen, and Terry M. Peters. Hologram stability evaluation for microsoft (r) hololens tm. In *Intl. Conf. on Robotics and Automation (ICRA)*, pages 3–14, Marina Bay Sands, Singapur, 2017. 2

[76] Florian Walch, Daniel Cremers, Sebastian Hilsenbeck, Caner Hazirbas, and Laura Leal-Taix. "Deep Learning for Image-Based Localization". Master's thesis, Technische Universität München, Department of Informatics, Semantic Scholar, Munich, Germany, 2016. 2

[77] Florian Walch, Caner Hazirbas, Laura Leal-Taixé, Torsten Sattler, Sebastian Hilsenbeck, and Daniel Cremers. "Image-Based Localization Using LSTMs for Structured Feature

Correlation". In *Intl. Conf. on Computer Vision (ICCV)*, pages 627–637, Venice, Italy, 2017. 1, 2, 4, 5, 6, 7, 8

[78] Junqiu Wang, Hongbin Zha, and Roberto Cipolla. "Coarse-to-Fine Vision-Based Localization by Indexing Scale-Invariant Features". In *Trans. on Systems, Man, and Cybernetics*, volume 36(2), pages 413–422, Apr. 2006. 2

[79] Sen Wang, Ronald Clark, Hongkai Wen, and Niki Trigoni. "DeepVO: Towards end-to-end Visual Odometry with deep Recurrent Convolutional Neural Networks". In *Intl. Conf. on Robotics and Automation (ICRA)*, pages 2043–2050, Singapore, Singapore, 2017. 2, 8

[80] Qi Zhao, Fangmin Li, and Xinhua Liu. "Real-time Visual Odometry based on Optical Flow and Depth Learning". In *Intl. Conf. on Measuring Technology and Mechatronics Automation (ICMTMA)*, pages 239–242, Changsha, China, 2018. 3